045

Journal of Microscopy, Vol. 183, Pt 3, September 1996, pp. 197–204.
Received 20 October 1995; accepted 26 April 1996

Two-photon excited lifetime imaging of autofluorescence in cells during UVA and NIR photostress

K. KÖNIG,*† P. T. C. SO,‡ W. W. MANTULIN,‡ B. J. TROMBERG§ & E. GRATTON‡
*Institute of Anatomy II, Friedrich Schiller University, Teichgraben 7, D-07743 Jena, Germany
†Institute of Molecular Biotechnology, Jena, Germany
‡LFD, Department of Physics, University of Illinois, Urbana, IL, USA
§Beckman Laser Institute and Medical Clinic, University of California, Irvine, CA, USA

Key words. Femtosecond pulses, laser microscopy, lifetime imaging, NADH, near-infrared, time-resolved fluorescence, two-photon excited fluorescence.

Summary

By monitoring coenzyme autofluorescence modifications, as an indicator of cell damage, the cellular response to femtosecond near-infrared (NIR) radiation (two-photon absorption) was compared with exposure to low-power UVA radiation (one-photon absorption). Excitation radiation from a tunable Ti-sapphire laser, focused through high-numerical-aperture microscope optics, provided diffraction-limited microbeams of an adjustable peak power. Laser scanning NIR microscopy was used to detect spatially the intracellular distribution of fluorescent coenzymes by fluorescence intensity imaging as well as fluorescence lifetime imaging (τ-mapping).

Upon the onset of UV or NIR exposure, Chinese hamster ovary cells exhibited blue/green autofluorescence with a mean lifetime of 2·2 ns, which was attributed to NAD(P)H in mitochondria. Exposure to 365 nm radiation from a high-pressure mercury lamp (1 mW, 300 J cm^{-2}) resulted in oxidative stress correlated with increased autofluorescence intensity, onset of nuclear fluorescence, and a fluorescence lifetime decrease. The cellular response to femtosecond NIR microbeams depended significantly on peak power. Peak powers above a threshold value of about 0·5 kW (average power: 6 mW), 0·55 kW (7 mW) and 0·8 kW (10 mW) at 730 nm, 760 nm and 800 nm, respectively, resulted in the onset of short-lived luminescence with higher intensity (100×) than the intracellular NAD(P)H fluorescence. This luminescence, accompanied by destruction of cellular morphology, was localized and occurred in the mitochondrial region. In contrast, beams at a power of less than 0·5 kW allowed nondestructive fluorophore detection with high spatial and temporal resolution without modification of cellular redox state or cell morphology.

Correspondence to: K. König. Tel. +49 3641631820; Fax +49 3641631249; e-mail: kkoe@mti-n.uni-jena.de

Introduction

We describe time-resolved autofluorescence measurements on individual living cells, using a two-photon scanning microscope for fluorescence intensity and fluorescence lifetime imaging. Intracellular autofluorescence originates from endogenous fluorophores such as the fluorescent reduced coenzymes β-nicotinamide adenine dinucleotide (NADH) and β-nicotinamide adenine dinucleotide phosphate (NADPH), denoted here as NAD(P)H. Free NAD(P)H absorbs in the ultraviolet region around 340 nm with a fluorescence maximum near 460 nm and a mean lifetime of ≈400 ps. Bound NAD(P)H exhibits a blue-shifted fluorescence maximum of 440 nm and a fluorescence decay time around 2 ns (Schneckenburger & König, 1992). The NAD(P)H fluorescence acts as indicator for cellular metabolism and reflects the intracellular redox state (Chance & Thorell, 1959; Schneckenburger & König, 1992; König & Schneckenburger, 1994). We monitored modifications of cellular autofluorescence to obtain information on possible pathophysiological effects induced by UVA exposure and near-infrared (NIR) femtosecond excitation pulses. In two-photon excitation NIR microscopy, excitation of UV/blue absorbing chromophores occurs only at the focal spot, in contrast to conventional one-photon laser scanning microscopes, where excitation occurs throughout the illumination cone. The two-photon spot excitation reduces overall photobleaching/photodamage. Furthermore, damage of unstained cells is not expected to occur in out-of-focus regions, since cellular absorption of NIR absorption is minimal. However, there are no detailed studies on photodamage induced by highly focused ultrashort NIR pulses. Risdale & Webb (1993) reported that cell damage occurred between 40 and 75 mW (no wavelengths are given) during two-photon laser scanning microscopy. Cell killing of myocytes induced by femtosecond NIR pulses was found at 15 mW (Piston *et al.*, 1994). NAD(P)H in rabbit

eyes was imaged with 15 mW, highly focused femtosecond beams at 705 nm without photoinduced cell damage (Piston *et al.*, 1995).

We used intensity and lifetime imaging of cellular autofluorescence to examine the sensitivity of our two-photon microscope, for detecting possible pathophysiological effects of the pulsed NIR excitation beam, and to establish the limits of two-photon microscopy as a nondestructive tool for vital cell imaging. In particular, we used the microscope to investigate and quantify modifications in cellular autofluorescence patterns and lifetime during UVA exposure (one-photon absorption) in comparison with 730–800 nm exposure (two-photon absorption). Both types of exposure result in excitation of UVA transitions of endogenous cellular chromophores. In addition to generation of autofluorescence, type I and type II photon-oxidation processes can be induced, resulting in oxidative stress and cell death (Cunningham *et al.*, 1985; Tyrell & Keyse, 1990; König *et al.*, 1995b).

Two-photon excitation

The feasibility of multi-photon excitation of electronic states was predicted by Göppert-Meyer (1931), first realized with the availability of lasers in 1961 (Kaiser & Garrett, 1961) and applied to two-photon excitation laser microscopy in 1990 (Denk *et al.*, 1990). As schematically shown in Fig. 1, two-photon excitation may occur by simultaneous absorption of two photons either of different photon energy or of the same energy. Due to a relatively low molecular cross-section of about 10^{-48}–10^{-50} cm^4 s^{-1} (Hermann & Ducuing, 1972; Kennedy & Lytle, 1986), two-photon excitation requires high photon flux. As demonstrated recently (Hänninen *et al.*, 1994; König *et al.*, 1995a), intracellular two-photon fluorescence can be obtained with highly focused continuous wave (cw) laser beams. For example, the photon flux density in a diffraction-limited 100-mW, NIR cw-laser microbeam of about 10^{26} photons cm^{-2} s^{-1} is sufficient for two-photon excitation. Thus, for probes with quantum yields ≈ 1, fluorescence signals of 10^2–10^4 photons s^{-1} per molecule can be generated in a 300-nm × 300-nm × 900-nm spot ($\approx 0{\cdot}1\ \mu m^3$ excitation volume). For 10^{-5} M dyes ($\approx$600 molecules in the excitation volume) and instrument efficiencies of the order of 1%, this corresponds to detector count rates of the order of 10^3–10^5 s^{-1}. These signal levels can be measured using a variety of commercially available detector systems and are generally in the range of ocular sensitivity.

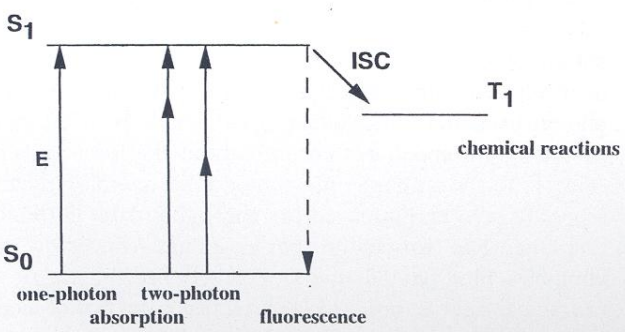

Fig. 1. Schematic representation of one-photon and two-photon excitation processes. The energy E to occupy the first electronic state (S_1) can be provided by photons of high photon energy E_p with $E_p = E$, or by simultaneous absorption of two low-energy photons with $E_{p1} + E_{p2} = E$. In the case of single-beam two-photon microscopes, the two photons have the same energy ($E_{p1} = E_{p2}$), although this condition is not required.

In practice, higher photon fluxes are necessary to achieve two-photon fluorescence imaging with a reasonable frame rate. In particular, high fluxes are required when imaging fluorophores with a low fluorescence quantum yield. An increase in cw power induces thermal and photochemical damage in seconds (Liu *et al.*, 1995; König *et al.*, 1995a). For example, an intracellular temperature increase of 1–2 K per 100 mW was measured for 1064-nm microbeams. By contrast, using a pulsed laser microbeam, efficient multi-photon-excitation can be achieved with peak powers in the watt and kilowatt range but average power in the milliwatt range. Appropriate laser sources include mode-locked, tunable Ti:sapphire lasers (700–1000 nm), which provide femtosecond pulses with a high repetition frequency. Fluorophores with one-photon absorption bands in the range 350–500 nm can be excited by the Ti:sapphire laser in the two-photon mode. It should be noted that two-photon excitation spectra may differ from one-photon fluorescence excitation spectra with the wavelength axis doubled (Kennedy & Lytle, 1986). In addition to fluorescence intensity measurements, the application of ultrashort excitation pulses allows fluorescence lifetime measurements. Two-photon microbeam scanning in combination with frequency domain heterodyning technique allow time-resolved fluorescence imaging (τ-mapping) to be performed in microscopes (Piston *et al.*, 1992; So *et al.*, 1995).

Materials and methods

Experimental set-up

The NIR excitation pulses for the two-photon laser scanning microscope (modified inverted fluorescence microscope Axiovert 35, Zeiss) were provided by an Ar$^+$-ion-laser pumped, passively mode-locked Ti:sapphite laser (Innova 310, Mira 900, Coherent) operating at a pulse width of 150 fs and a repetition frequency of 80 MHz (Fig. 2). The attenuated and expanded excitation beam was directed by 1-kHz x,y-scanner-mirrors (Model: 6350, Cambridge Technology) and focused to a diffraction-limited spot by a 63× Plan-Neofluar objective (numerical aperture: 1·25)

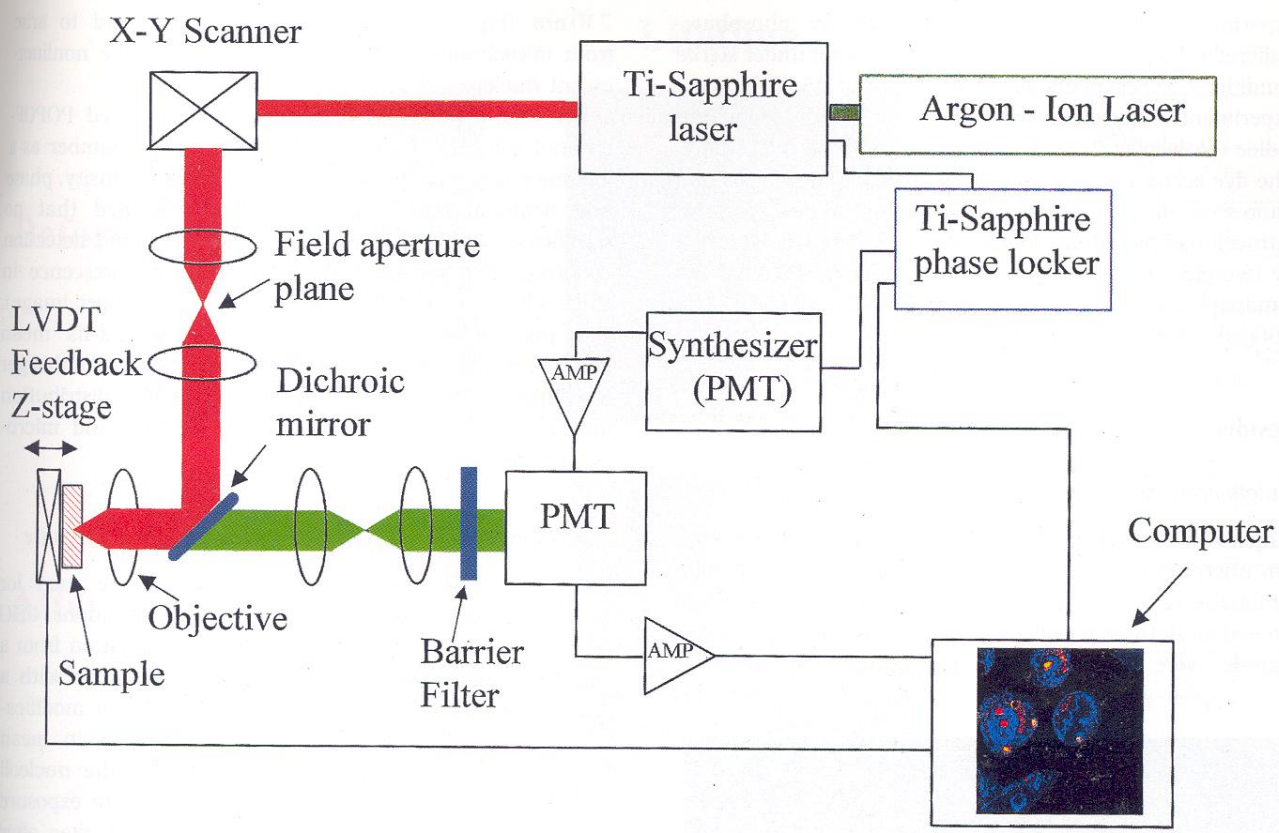

Fig. 2. Experimental set-up. The tunable, mode-locked Ti:sapphire laser, excited by the argon-ion laser, provides the femtosecond excitation pulses. The expanded, x, y-scanning NIR beam is focused by a 63× objective and excites visible fluorescence in a submicrometre-sized sample region. The NIR-excited fluorescence is detected by a modulated PMT. The laser source, detection system and computer comprise a phase locked loop. Image processing allows intensity-, phase shift- and demodulation-imaging.

Autofluorescence was collected by the same objective, transmitted through a dichroic mirror FT 650 and refocused on a modified, 80·025-MHz modulated R928 PMT (Hamamatsu) equipped with SP 550 filters. POPOP with a decay time of 1·3 ns in ethanol served as the reference material in frequency-domain heterodyne measurements. Illumination power was adjusted with a Glan-Thompson polarizer. A $\lambda/4$ plate provided circular polarized excitation radiation. The mean laser power was measured with a power meter (Newport Powermeter, model 1825-C) after the objective at the sample plane. The two-photon laser scanning microscope, including the imaging processing software, has been described in detail (So *et al.*, 1995).

In all the experiments, we used a frame rate of 10 s. The pixel dwell time was 80 μs with a waiting time of ≈6 s between consecutive frames. Fluorescence was detected in a field of $35 \times 35\ \mu m^2$ (using 63×, 1·25-NA objective, 256 × 256 pixels). A peak power of 0·8 kW was estimated for 10 mW mean power (150 fs pulse with a 80-MHz repetition frequency). We experimentally determined a FWHM beam size at the focal spot or 0·25 μm at 730 nm (for experiment details see So *et al.*, 1995). For each scanning point the intensity and radiant exposure at the sample during one scan were 1·6 TW cm^{-2} and 2 kJ cm^{-2}, respectively (0·8-kW pulses). Three wavelengths (730, 760 and 800 nm) spanning the tuning range of the first mirror set of the laser resonator were chosen. The NIR wavelength range up to 800 nm is of special interest due to possible excitation of UV absorbers and the strongest influence on cell viability. Today, most two-photon studies are performed in this wavelength range.

One-photon UVA radiation (1·5 mW after the 100× objective; wide-field illumination; 5 W cm^{-2}) was provided by a 50-W high-pressure mercury lamp (Oriel) equipped with a 365 ± 25-nm bandpass and a heat protection filter.

Cells

Chinese hamster (*Cricetulus griseus*) ovary cells (CHO, ATCC no. 61) were maintained in Gibco's minimum essential medium (MEM, 10% fetal bovine serum). Cells were subcultured in T-25 tissue culture flasks twice a week. Fifteen hours prior to experiment, cells were injected into a modified Rose culture chamber. For the microscope

experiment, the medium was replaced by phosphate-buffered saline (PBS, pH = 7·4). Cells were kept under sterile conditions. Experiments were carried out at 25 °C. In some experiments, the fluorescent dead-cell stain, propidium iodide (Molecular Probes), was added to probe cell vitality. The dye accumulates in nucleic acids of damaged cells and fluoresces in the red spectral range. When present, intracellular propidium iodide accumulation was detected by two-photon excited fluorescence using a 650 ± 20-nm bandpass filter (no short-pass filters; excitation with 730-, 760- and 800-nm pulses).

Results

Autofluorescence imaging

Single CHO cells were scanned with 730-, 760- and 800-nm microbeams. Simultaneously, autofluorescence modifications were monitored. Blue/green autofluorescence was excited at all three wavelengths. The strongest fluorescence signals were obtained with two-photon excitation at 730 nm (Fig. 3). Autofluorescence was found to arise from mitochondria, mainly located around the nonfluorescent nucleus.

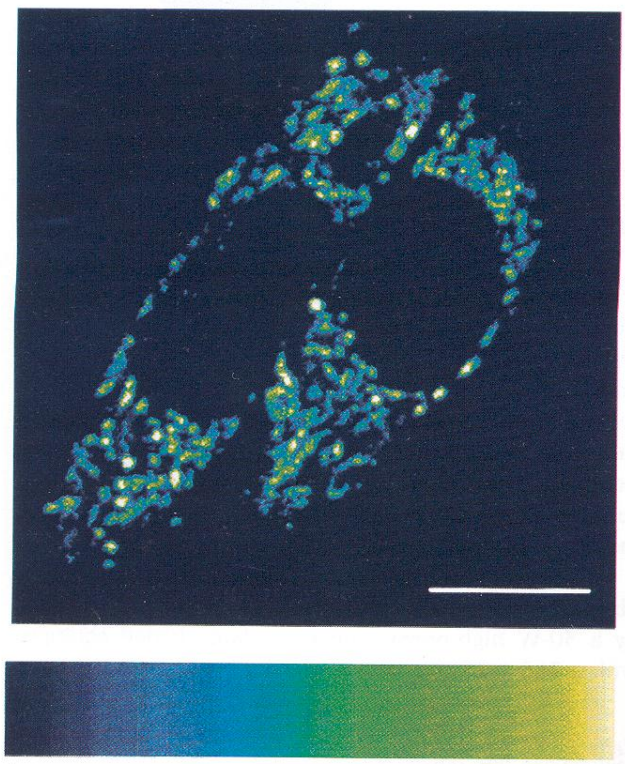

Fig. 3. Autofluorescence imaging of a single CHO cell excited with 730-nm pulses (average power: 2 mW). Autofluorescence is mainly from NAD(P)H-containing mitochondria. The nucleus is nonfluorescent. The scale bar indicates a length of 10 μm.

For time-resolved imaging, we first measured POPOP-ethanol solution (1·3 ns lifetime) in a Rose chamber as a lifetime reference. The nearly homogeneous intensity, phase and demodulation image of POPOP indicated that no significant spatial dependence of excitation and detection occurred. The spatial distribution of autofluorescence in CHO cells ('τ-mapping') is shown in Fig. 4 (upper image). The pixel lifetime histogram presents a 2·2-ns mean lifetime, which is typical for NAD(P)H (Schneckenburger & König, 1992). The width of the lifetime distribution indicates heterogeneous fluorophore binding and microenvironments.

Autofluorescence modifications induced by UVA exposure

Laser microbeams of 4 mW at 730 nm were used for probing UVA-induced autofluorescence modifications. CHO cells were exposed to low-power 365-nm radiation from a mercury lamp (one-photon absorption). Exposure with a radiant exposure of 300 J cm^{-2} led to significant modifications in autofluorescence patterns, as well as in mean lifetime, Fig. 4 (lower image). Interestingly, the nucleoli which showed no fluorescence emission prior to exposure became the brightest intracellular fluorescent sites after UVA exposure. The mean cellular fluorescence intensity increased about 60-fold compared with nonexposed cells. The changes in the intensity-images were accompanied by modifications in lifetime distribution. In particular, the centre of the lifetime distribution shifted from 2·2 to 1·8 ns. The nucleoli exhibited the same lifetime as the cytoplasm.

Luminescence modifications induced by NIR exposure

We increased the mean power of the 730-nm excitation beam to a value of 6 mW (0·5 kW peak power) and repeatedly scanned individual cells 10 times at 16-s time intervals. Figure 5 demonstrates the typical luminescence behaviour. The first scan of three cells revealed an intensity pattern similar to that seen in Fig. 3. Interestingly, the third scan of exactly the same cellular areas 32 s after the first scan revealed modifications in the cellular luminescence pattern. In particular, a small intracellular region near the nucleus of two cells showed increased intensity. Further scanning resulted in a continued signal increase (up to 200-fold) and in enlargement of the previously induced luminescent area. The highly luminescent areas were also visible with the eye (using the eyepieces, replacement of SP550 by SP650 short-pass filter) as 'white' flashes during illumination with the scanning beam. All cells ($n = 20$) showed a similar pattern of increasing luminescence. However, the onset of luminescence occurred at different

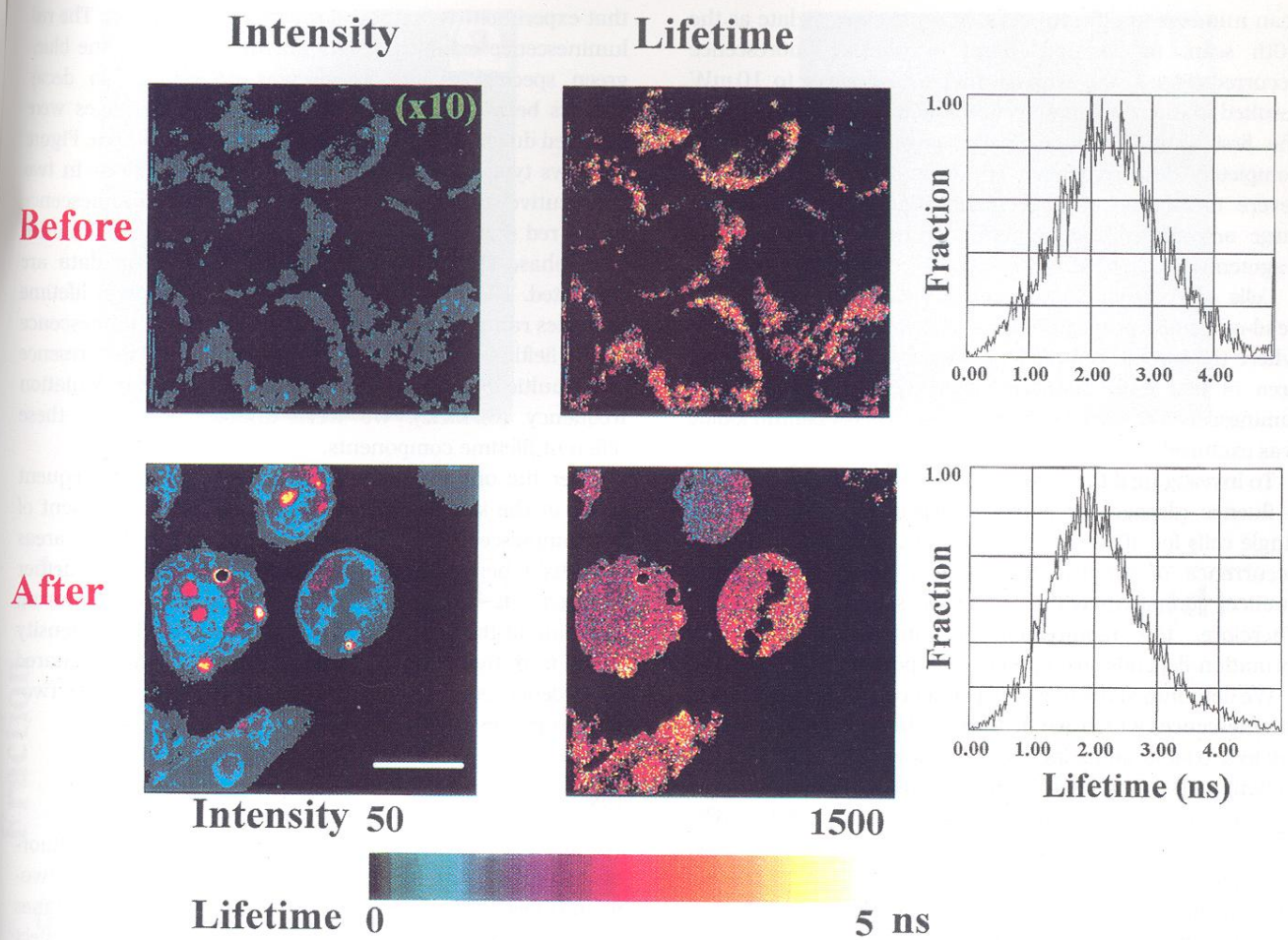

Fig. 4. Intensity imaging and lifetime imaging of CHO autofluorescence (730 nm, 4 mW average power) prior to (upper image) and after (lower image) low-power UVA stress. UVA exposure (one-photon absorption) produces intense autofluorescence, fluorescence relocalization, onset of nuclear fluorescence and a decrease in lifetime (see lifetime histogram). Lifetimes were calculated from demodulation data. The black regions are pixels below a certain intensity threshold. The vertical axis of the lifetime histogram represents the fraction of valid pixels. The white scale bar indicates a length of 10 μm.

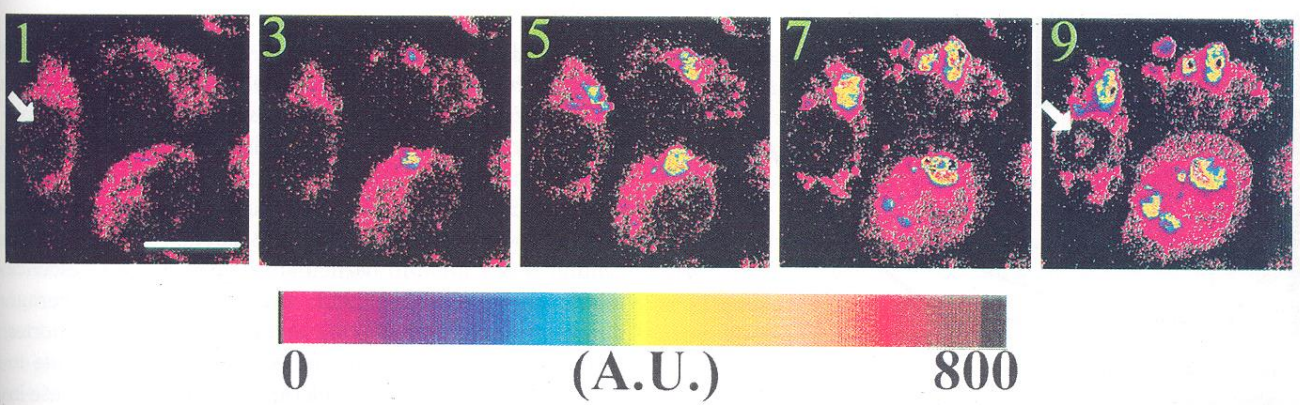

Fig. 5. Modifications of cellular luminescence induced by a 730-nm excitation beam at an average power of 6 mW as a function of the number of scans. Onset of intense luminescence occurred in the mitochondrial region. Arrows indicate formation of nuclear fluorescence. The white scale bar represents a length of 10 μm.

scan numbers in different cells, in some cases as late as the 10th scan. In addition, onset of nuclear fluorescence occurred (Fig. 5, see arrows). Increasing power to 10 mW resulted in intense luminescence which always started with the first scan. Morphologically, most of the cells were completely destroyed after 10 scans. These cells showed severe membrane damage (membrane blebbing), loss of large amounts of cell material, or even disruption into fragments.

Cells with strong luminescence were permeable to the dead-cell stain propidium iodide. However, in some cells where the luminescent spot was localized in a cytoplasmic area of less than 2 μm diameter (cells where onset of luminescence occurred with scan 9 or 10), propidium iodide was excluded.

To investigate if the onset of luminescence followed either a fluence (dosage) or a power dependence, we scanned single cells for 30 min (180 scans) at 2 mW. There was no occurrence of intense luminescence in spite of higher fluence compared with 10 times scanning at 6 mW. Therefore, the requirement for intense luminescence formation depends strongly on peak power levels.

We determined the power dependence for the onset of this luminescence, which we defined as the power corresponding to a 10-fold signal increase. As shown in Fig. 6, 730-nm radiation of 4, 6 and 8 mW induced intense luminescence in 10, 50 and 100% of the cells ($n = 20$), respectively. The threshold, which we defined as the power at which 50% of cells showed intense luminescence, was 6 mW (730 nm). Intense luminescence was also induced by pulses at 760 and 800 nm at other power levels. As seen from Fig. 6, we found higher threshold values at 760 nm excitation (7 mW) and at 800 nm (10 mW).

Luminescence was not limited to the blue/green spectral region. Intense luminescence was also detected in the red spectral region using a 650 ± 20-nm bandpass filter (for

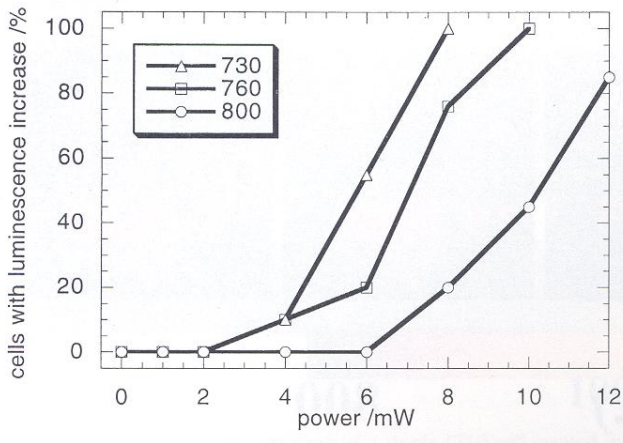

Fig. 6. Percentage of cells which show onset of intense luminescence as a function of average laser power ($n = 20$ cells, 10 scans) and excitation wavelengths.

that experiment we removed the short-pass filters). The red luminescence exhibited decay kinetics similar to the blue/green spectral region. There was no change in decay kinetics between successive scans, although images were modified due to enlargement of the luminescent area. Figure 7 shows typical cellular luminescence distributions in two consecutive scans of a single cell with intense luminescence in the red region. In addition, lifetime histograms obtained from phase shift as well as from demodulation data are presented. The difference in phase and modulation lifetime indicates rather complex decay kinetics of the luminescence with a lieftime in the subnanosecond region and the presence of a multiexponential decay. Using only one modulation frequency (80 MHz), we were unable to resolve these different lifetime components.

After the onset of intense luminescence, all subsequent scans at the same power levels lead to an enlargement of the luminescent area. The luminescent intracellular areas persisted when the power was reduced to 1 mW. No further enlargement of the luminescent area occurred during scanning at this low power (data not shown). The intensity signal from the luminescent areas showed a nearly squared dependence on power ($R = 0{\cdot}97$) as expected for a two-photon process.

Discussion

We have demonstrated (time-resolved) detection of fluorescent coenzymes in single cells, using a sensitive two-photon laser scanning microscope. Using these coenzymes as bioindicators of cellular metabolism, we studied the effect of UVA and NIR photostress by monitoring autofluorescence. Typical radiant exposures for cell-killing effects induced by cw NIR microbeams were determined to be several GJ cm^{-2} (optically trapped spermatozoa, 760 nm). These destructive effects were accompanied by an increase of autofluorescence (König *et al.*, 1995a). Due to two-photon absorption, UVA-like biological effects may occur when NIR microbeams are used (König *et al.*, 1995a).

We used two-photon imaging at 4 mW average power to probe alterations in cellular autofluorescence after one-photon UVA absorption (exposure with mercury lamp). It is well known that UVA exposure induces oxidative stress (Cunningham *et al.*, 1985; Tyrell & Keyse, 1990; König *et al.*, 1995b). We found evidence for significant changes in autofluorescence, which indicate modifications in the cellular redox state. In particular, we detected fluorescence relocalization combined with a decrease in the average fluorescence lifetime. Free NAD(P)H exhibits a shorter lifetime (≈400 ps) than bound NAD(P)H (≈ 2 ns). Due to the decrease in the average lifetime, the general increase in autofluorescence could only be accounted for by an absolute intracellular increase of free NAD(P)H and/or a less tight protein binding. This result supports recent

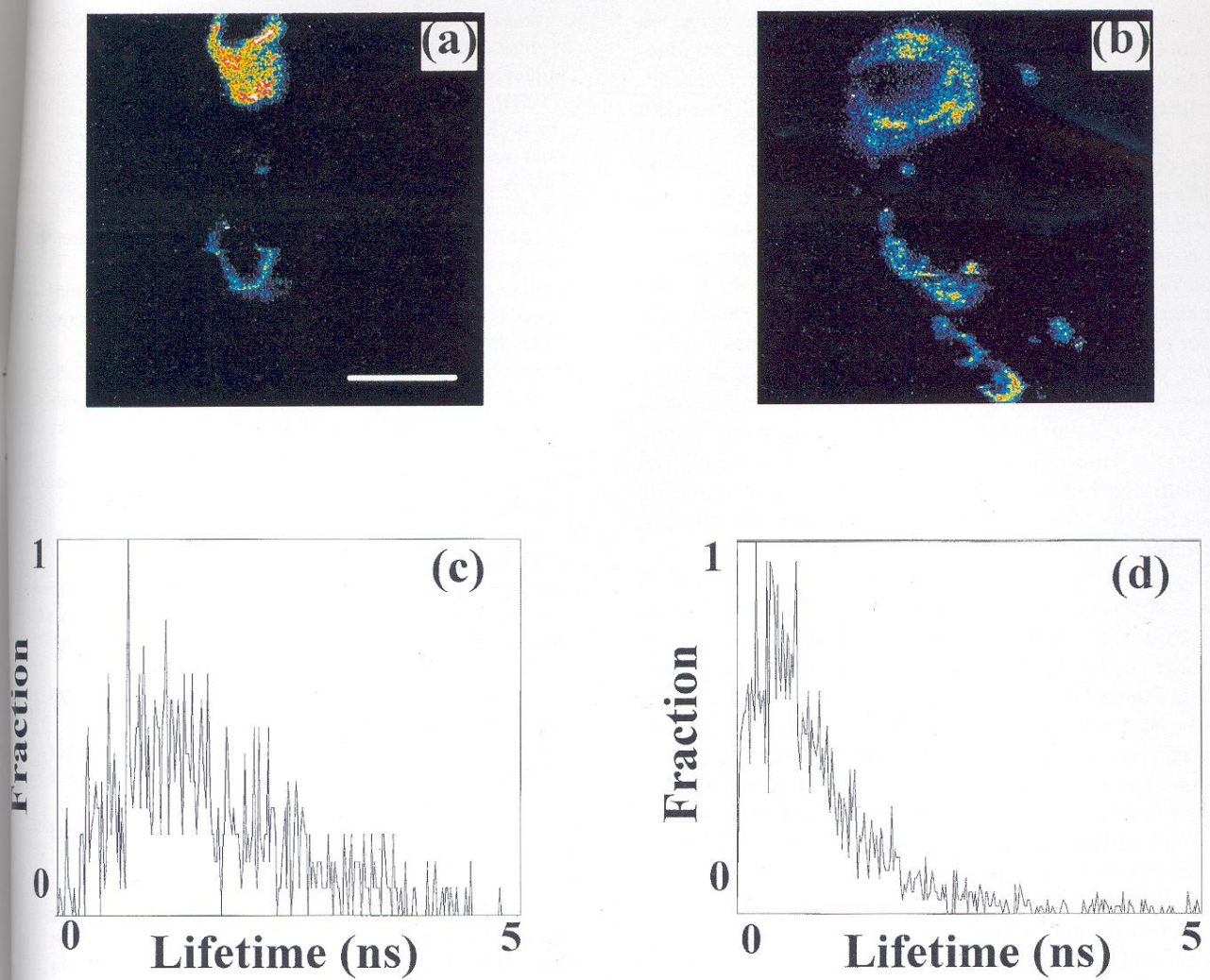

Fig. 7. Imaging of the intense luminescence in a CHO cell in the red spectral region (excitation wavelength: 760 nm, average power: 8 mW, emission filter: 650 ± 20 nm). Images (a) and (b) show the modification of fluorescent region upon two consecutive scans. Phase (c) and demodulation (d) lifetime histograms are obtained from data corresponding to image (a). Luminescence lifetime is not altered upon subsequent scans. The white scale bar indicates a length of 10 μm.

findings of UVA-induced intracellular red shifts in autofluorescence maxima (König *et al.*, 1995b).

One possible explanation for the autofluorescence increase is UVA-induced formation of reactive oxygen species via type I and II photo-oxidation with intracellular coenzymes and porphyrins as photosensitizers (Cunningham *et al.*, 1985; Tyrell & Keyse, 1990). These reactive species may induce damage to the mitochondrial membrane and, therefore, NAD(P)H efflux from mitochondria into the cytosol. A portion of the cytosolic NAD(P)H may penetrate through the nuclear membrane and bind to protein-rich nucleoli. In addition, enhanced biosynthesis of NAD(P)H may occur.

In this study, we found that application of femtosecond NIR pulses may influence cellular metabolism. However, pulse powers of 0·3 kW or less and pixel dwell times in the microsecond range did not induce significant modifications to cellular autofluorescence or to cell morphology.

We found that 10 scans of NIR excitation pulses of higher peak power (≈1 kW) can induce autofluorescence changes similar to those arising from low-power UVA light. In particular, we were able to detect nuclear autofluorescence (see Fig. 5). However, these autofluorescence changes are accompanied by another more destructive effect. NIR pulses above threshold powers of about 0·5 kW (730 m), 0·55 kW (760 nm) and 0·8 kW (800 nm) induced intracellular localized luminescence in most of the cells. These high photon fluxes could be sufficient to create intracellular plasma formation. The formation of highly luminescent spots always occurred around the nucleus, in the region of

high mitochondrial concentration. Therefore, the formation of intense luminescence seems to be dependent on mitochondrial absorbers. Clearly, luminescence onset depends on peak power. However, the luminescence enhancement does not always appear with the first scan, which could imply a memory effect. We propose that the scanning beam induces a change in the optical properties (absorption coefficient, scattering coefficient, dielectric constant) somehow providing conditions propitious for the generation of optical breakdown within the cell. After onset of the intense luminescence, further damage becomes more likely and strong fluorescence signals persist even after power reduction, perhaps as a result of photoinduced modifications. These modifications may result in photoinduced formation of unknown fluorescent products, e.g. protein photoproducts. However, photoproduct formation would not explain the severe morphological cell damage observed. As mentioned, the strong luminescence in CHO cells was accompanied by cell destruction.

Recently, the generation of strong luminescent spots in dye solutions during exposure with 750-nm femtosecond pulses of 0·75 TW cm^{-2} peak intensity has been reported (Hell *et al.*, 1995). These authors suggest that their signal arises from a laser-induced fluorophore deposition onto the cover slip surface. Unfortunately, they provide no data (spectral or lifetime) that the observed luminescent spot can be characterized as fluorescence. Further studies are necessary to explain the origin of the intense luminescence.

In conclusion, two-photon microscopes provide sensitive, nondestructive tools in vital cell microscopy. We have determined the experimental limits for live cell imaging with the most common two-photon microscopy parameters (pulse width of the order of 150 fs and repetition rate of the order of 80 MHz). Vital cell imaging can be performed with NIR excitation with peak power kept below threshold values in the 0·3 kW range (730–800 nm). In two-photon microscopy, one must continually remain cognisant of the potential for cell damage. Future studies are planned with more sensitive cloning assays to determine long-term genetic damage. We will further investigate the relationship between NIR laser source pulse width and repetition rate as well as the damaging potential of longer NIR radiation (800–1000 nm).

Acknowledgments

This work was supported by the Deutsche Forschungsgesellschaft, by the National Institutes of Health (RR03155 and RR01192), and by the Department of Energy (DE-FG391ER61227).

References

Chance, B. & Thorell, B. (1959) Localization and kinetics of reduced pyridine nucleotides in living cells by microfluorimetry. *J. Biol. Chem.* **234**, 3044–3050.

Cunningham, M.L., Johnson, J.S., Giovanazzi, S.M. & Peak, M.J. (1985) Photosensitized production of superoxide anion by monochromatic (290–405 nm) ultraviolet irradiation of NADH and NADPH coenzymes. *Photochem. Photobiol.* **42**, 125–128.

Denk, W., Strickler, J.H. & Webb, W.W. (1990) Two-photon laser scanning fluorescence microscope. *Science*, **248**, 73–76.

Göppert-Meyer, M. (1931) Über Elementarakte in zwei Quantensprüngen. *Ann. Phys.* **9**, 273.

Hänninen, P.E. Soini, E. & Hell, S.W. (1994) Continuous wave excitation two-photon fluorescence microscopy. *J. Microsc.* **176**, 222–225.

Hell, S.W., Utz, A.R., Schrader, M., Hänninen, P.E. & Soini, E. (1995) Pulsed laser fluorophore deposition: a method for measuring the axial resolution in two-photon fluorescence microscopy. *J. Opt. Soc. Am.* **A12**, 2072–2076.

Hermann, J.P. & Ducuing, J. (1972) Absolute measurements of two-photon cross sections. *Phys. Rev.* **A5**, 2557–2568.

Kaiser, W. & Garrett, C.G.B. (1961) Two-photon excitation in CaF_2:Eu^{2+}. *Phys. Rev. Lett.* **7**, 229–231.

Kennedy, S.M. & Lytle, F.E. (1986) P-Bis(o-methylstyryl)benzene as a power squared tensor for two-photon absorption measurements between 537 and 694 nm. *Anal. Chem.* **58**, 2643–2647.

König, K., Hong, L., Berns, M.W. & Tromberg, B.J. (1995a) Cell damage by near-IR microbeams. *Nature*, **377**, 20–21.

König, K., Liu, Y., Sonek, G.J., Berns, M.W. & Tromberg, B.J. (1995b) Autofluorescence Spectroscopy of optically trapped cells. *Photochem. Photobiol.* **62**, 830–835.

König, K. & Schneckenburger, H. (1994) Laser-Induced autofluorescence for medical diagnosis. *J. Fluorescence*, **4**, 17–40.

Liu, Y., Cheng, D., Sonek, G.J., Berns, M.W., Chapman, C.F. & Tromberg, B.J. (1995) Evidence for localized cell heating induced by infrared optical tweezers. *Biophys. J.* **68**, 2137–2144.

Piston, D.W., Kirby, M.S., Cheng, H. & Lederer, W.J. (1994) Two-photon excitation fluorescence imaging of three-dimensional calcium-ion activity. *Appl. Opt.* **33**, 662.

Piston, D.W., Masters, B.R. & Webb, W.W. (1995) Three-dimensionally resolved NAD(P)H cellular metabolic redox imaging of the *in situ* cornea with two-photon excitation laser scanning microscopy. *J. Microsc.* **178**, 20–27.

Piston, D.W., Sandison, D.R. & Webb, W.W. (1992) Time resolved fluorescence imaging and background rejection by two-photon excitation in laser scanning microscopy. *Proc. SPIE*, **1640**, 379–389.

Risdale, J.A. & Webb, W.W. (1993) The viability of cultured cells under two-photon laser scanning microscopy. *Biophys. J.* **63**, A109.

Schneckenburger, H. & König, K. (1992) Fluorescence decay kinetics and imaging of NAD(P)H and flavins as metabolic indicators. *Opt. Eng.* **31**, 1447–1451.

So, P.T.C., French, T., Yu, W.M., Berland, K.M., Dong, C.Y. & Gratton, E. (1995) Time-resolved fluorescence microscopy using two-photon excitation. *Bioimaging*, **3**, 1–15.

Tyrell, R.M. & Keyse, S.M. (1990) The interaction of UVA radiation with cultured cells. *J. Photochem. Photobiol.* **4**, 349–361.